

Citation for published version:

Delgorio, PL, Hiscox, LV, Daugherty, AM, Sanjana, F, McIlvain, G, Pohlig, RT, McGarry, MDJ, Martens, C, Schwarb, H & Johnson, CL 2022, 'Structure-Function Dissociations of Human Hippocampal Subfield Stiffness and Memory Performance', *Journal of Neuroscience*, vol. 42, no. 42, pp. 7957-7968.
<https://doi.org/10.1523/JNEUROSCI.0592-22.2022>

DOI:

[10.1523/JNEUROSCI.0592-22.2022](https://doi.org/10.1523/JNEUROSCI.0592-22.2022)

Publication date:

2022

Document Version

Peer reviewed version

[Link to publication](#)

University of Bath

Alternative formats

If you require this document in an alternative format, please contact:
openaccess@bath.ac.uk

General rights

Copyright and moral rights for the publications made accessible in the public portal are retained by the authors and/or other copyright owners and it is a condition of accessing publications that users recognise and abide by the legal requirements associated with these rights.

Take down policy

If you believe that this document breaches copyright please contact us providing details, and we will remove access to the work immediately and investigate your claim.

1 **Title:** Structure-Function Dissociations of Human Hippocampal Subfield Stiffness and Memory
2 Performance

3 **Abbreviated Title:** Hippocampal Subfield Stiffness and Memory Function
4

5 Peyton L Delgorio¹, Lucy V Hiscox¹, Ana M Daugherty², Faria Sanjana³, Grace McIlvain¹, Ryan
6 T Pohlig⁴, Matthew DJ McGarry⁵, Christopher R Martens³, Hillary Schwarb⁶, Curtis L Johnson¹
7

8 1 Department of Biomedical Engineering, University of Delaware, Newark, DE, 19716, USA

9 2 Department of Psychology and Institute of Gerontology, Wayne State University, Detroit,
10 MI, 48202, USA

11 3 Department of Kinesiology and Applied Physiology, University of Delaware, Newark, DE,
12 19713, USA

13 4 Biostatistics Core Facility, College of Health Sciences, University of Delaware, Newark, DE,
14 19716, USA

15 5 Thayer School of Engineering, Dartmouth College, Hanover, NH, 03755, USA

16 6 Beckman Institute for Advanced Science and Technology, University of Illinois at Urbana-
17 Champaign, Urbana, IL, 61801, USA
18

19 **Correspondence to:** Curtis L Johnson, clj@udel.edu
20

21 **Text Pages:** 34

22 **Figures:** 6

23 **Tables:** 6

24 **Words:** **Abstract:** 240

25 **Introduction:** 648

26 **Discussion:** 1498
27

28 **Financial Interests or Conflicts of Interest:** We have no financial interests or conflicts of
29 interest to disclose.
30

31 **Acknowledgements:** This research was supported by grants from the National Institutes of
32 Health (R01-AG058853, R01-EB027577, K01-AG054731, and R03-AG065894), Delaware
33 INBRE (P20-GM103446), Delaware Cardiovascular COBRE (P20-GM113125), and Delaware
34 Neuroscience COBRE (P20-GM103653).

35 **Abstract**

36 Aging and neurodegenerative diseases lead to decline in thinking and memory ability.
37 The subfields of the hippocampus (HCsf) play important roles in memory formation and recall.
38 Imaging techniques sensitive to the underlying HCsf tissue microstructure can reveal unique
39 structure-function associations and their vulnerability in aging and disease. The goal of this study
40 was to use magnetic resonance elastography (MRE), a noninvasive MR imaging-based technique
41 that can quantitatively image the viscoelastic mechanical properties of tissue, to determine the
42 associations of HCsf stiffness with different cognitive domains across the lifespan. 88 adult
43 participants completed the study (age: 23-81 years, M/F 36/51), in which we aimed to determine
44 which HCsf regions most strongly correlated with different memory performance outcomes and
45 if viscoelasticity of specific HCsf regions mediated the relationship between age and
46 performance. Our results revealed that both interference cost on a verbal memory task and
47 relational memory task performance were significantly related to cornu ammonis 1-2 (CA1-
48 CA2) stiffness ($p = 0.018$ and $p = 0.011$, respectively), with CA1-CA2 stiffness significantly
49 mediating the relationship between age and interference cost performance ($p = 0.031$). There
50 were also significant associations between delayed free verbal recall performance and stiffness of
51 both the dentate gyrus-cornu ammonis 3 (DG-CA3) ($p = 0.016$) and subiculum (SUB) ($p =$
52 0.032) regions. This further exemplifies the functional specialization of HCsf in declarative
53 memory and the potential use of MRE measures as clinical biomarkers in assessing brain health
54 in aging and disease.

55

56

57

58
59
60
61
62
63
64
65
66
67
68
69
70
71
72
73
74
75
76
77
78
79

Significance Statement

Hippocampal subfields are cytoarchitecturally-unique structures involved in distinct aspects of memory processing. Magnetic resonance elastography is a technique that can noninvasively image tissue viscoelastic mechanical properties, potentially serving as sensitive biomarkers of aging and neurodegeneration related to functional outcomes. High-resolution *in vivo* imaging has invigorated interest in determining subfield functional specialization and their differential vulnerability in aging and disease. Applying MRE to probe subfield-specific cognitive correlates will indicate that measures of subfield stiffness can determine the integrity of structures supporting specific domains of memory performance. These findings will further validate our high-resolution MRE method and support the potential use of subfield stiffness measures as clinical biomarkers in classifying aging and disease states.

80

81 **Introduction**

82 The hippocampus (HC) is a brain structure involved in memory formation and
83 demonstrates structural decline in aging and neurodegenerative disease, such as Alzheimer's
84 disease (Morrison and Hof, 1997; Petersen et al., 2000). The individual subfields of the HC
85 (HCsf) (Duvernoy, 2005) include the dentate gyrus (DG), cornu ammonis sectors 1-3 (CA1-3),
86 and subiculum (SUB), which function together to retrieve, encode, and process memory (de
87 Flores et al., 2015). *In vivo* human imaging studies suggest the HCsf follow different trajectories
88 of decline in age and related disease, plausibly due to a differential decrease in neuron density
89 and myelin sheath degradation (West, 1993; Wisse et al., 2014; Daugherty et al., 2016).
90 Advanced age correlates with smaller HCsf volumes, and partially accounts for age-related
91 memory deficits in a region-specific manner as the HCsf each support distinct memory functions
92 (Mueller et al., 2007, 2011; Daugherty et al., 2016; Zammit et al., 2017). Whereas DG and CA3
93 correlate with relational memory performance, CA1 correlates with comparing current
94 experience to episodic recollection, while SUB is suggested to support memory integration and
95 delayed recall (Golomb et al., 1996; Leal and Yassa, 2018; Foster et al., 2019; Radhakrishnan et
96 al., 2020). However, evidence of specific structural correlates to memory function using gross
97 volumetric or diffusion MRI-based estimates leaves an open question of the underlying changes
98 in tissue microstructure. Imaging techniques sensitive to individual HCsf tissue integrity have the
99 potential to contribute to scientific understanding of the degeneration of these regions with age
100 and mechanisms of memory decline.

101 Magnetic resonance elastography (MRE) is a sensitive neuroimaging modality that can
102 provide reliable estimates of tissue viscoelastic mechanical properties (Hiscox et al., 2016). MRE

103 studies have shown changes in brain tissue viscoelasticity with aging (Hiscox et al., 2021) and in
104 neurodegenerative diseases (Murphy et al., 2019). Alterations in these properties are thought to
105 reflect biological changes in the microstructural composition and organization of the tissue (Sack
106 et al., 2013). Our group has previously observed strong relationships between HC viscoelasticity
107 and memory task performance in both young and older adults (Schwarb et al., 2016; Hiscox et
108 al., 2018), further highlighting that MRE metrics are functionally relevant, may provide insight
109 into memory performance decline across the lifespan, and are potential clinical biomarkers of
110 cognitive aging.

111 We recently developed a high-resolution MRE acquisition and analysis protocol to
112 reliably capture HCsf viscoelasticity. This MRE approach is the first to show differential age-
113 related effects between HCsf viscoelasticity (Delgorio et al., 2021) and allows us to further
114 explore individual HCsf mechanical structure-function relationships. One preliminary MRE
115 study found relational memory performance to be specifically related to DG-CA3 viscoelasticity
116 (Daugherty et al., 2020), suggesting that individual HCsf MRE measures may relate to different
117 aspects of memory performance, though this preliminary work used imaging and inversion
118 methods not optimized for examining the small HCsf. In this study, we use our higher resolution
119 MRE approach to better capture the unique structure-function relationships in the HCsf across
120 the lifespan, which may pave the way towards developing reliable clinical biomarkers related to
121 cognitive decline in both aging and disease.

122 The purpose of this study is to determine how HCsf viscoelasticity supports different
123 domains of memory, as quantified by performance on different cognitive tasks, by identifying if
124 relationships exist between individual HCsf MRE measures and memory performance metrics.
125 Based on previous studies, we hypothesize that CA1-CA2 viscoelasticity will associate with

126 recall following an interference (Mueller et al., 2011; Molitor et al., 2021), SUB viscoelasticity
127 will associate with delayed episodic recall (Travis et al., 2014; Zammit et al., 2017), and DG-
128 CA3 viscoelasticity will relate to relational memory (Azab et al., 2014; Daugherty et al., 2020).
129 Further, since both brain viscoelasticity and memory function change with age, we sought to
130 evaluate if HCsf mechanical metrics may characterize the microstructural variation partially
131 responsible for age-related differences in memory performance. We hypothesized that regional
132 HCsf viscoelasticity mediates the relation between age and associated task performance.

133

134 **Materials and Methods**

135 Eighty-eight participants were included from three different studies (age range: 23-81
136 years, M/F: 36/51); all participants completed identical one-hour MRI scanning protocols on a
137 3T Siemens Prisma MRI scanner. Subsets of these data have been previously reported (Delgorio
138 et al., 2021; Sanjana et al., 2021). We confirmed MRE data quality for each participant in our
139 sample, as quantified by octahedral shear strain signal-to-noise ratio (OSS-SNR), and all 88
140 participants had OSS-SNR values greater than the threshold of 3.0 necessary for stable property
141 estimation (McGarry et al., 2011; Hannum et al., 2021). Additionally, behavioral testing
142 marginally differed between studies such that not every participant completed every cognitive
143 task (see ‘Memory Assessment’ section below for more details).

144

145 High-Resolution MRE

146 Each MRI session included a high-resolution MRE acquisition and analysis protocol we
147 recently developed for examining the HCsf (Figure 1) (Delgorio et al., 2021). A commercial
148 Resoundant pneumatic driver (Resoundant, Rochester, MN) was used to apply 50 Hz acoustic

149 vibrations and induce brain tissue deformation on the micron scale. A 3D multiband, multishot
150 spiral MRE imaging sequence with 1.25 mm isotropic resolution was used to image the resulting
151 deformations (240x240 mm² field-of-view, 192x192 imaging matrix, 96 slices, 1.25 mm slice
152 thickness, TR/TE = 3360/70 ms) (Johnson et al., 2016a), which lasted approximately 10 minutes
153 and 45 seconds. Structural scans included a T₁-weighted magnetization prepared rapid
154 acquisition gradient echo (MPRAGE) scan at 0.9 mm isotropic resolution and a T₂-weighted
155 turbo spin echo (TSE) scan with 0.4x0.4x2.0 mm³ resolution aligned to the hippocampus, from
156 which Automated Segmentation of Hippocampal Subfields (ASHS) segmented each HCsf region
157 of interest: DG-CA3, CA1-CA2, and SUB (Yushkevich et al., 2015). FLIRT in FSL is used to
158 transform the subfield segmentations into MRE space to create binary masks of each HCsf
159 (Jenkinson et al., 2012). Finally, we used a nonlinear inversion algorithm (NLI) (McGarry et al.,
160 2012) to calculate tissue property measures from displacement data using the HCsf as spatial
161 priors through soft prior regularization (SPR) (McGarry et al., 2013). NLI is a finite-element
162 based inversion method that accounts for the heterogeneous nature of tissue and produces
163 reliable property images from data with sufficient OSS-SNR (McGarry et al., 2011). Reliability
164 of local property estimations can be further improved by providing anatomical information using
165 SPR (McGarry et al., 2013; Johnson et al., 2016b). NLI estimates the complex shear modulus
166 ($G = G' + iG''$), where G' is the storage modulus and G'' is the loss modulus. which is used to
167 compute the viscoelastic shear stiffness, $\mu = \frac{2|G|^2}{G' + |G|}$, and damping ratio, $\xi = \frac{G''}{2G'}$, that capture the
168 effective stiffness and attenuation, respectively. To maximize sensitivity and repeatability of
169 HCsf property estimates, we used NLI parameters optimized for HCsf with an SPR weighting of
170 $\alpha = 10^{-12}$ and two different spatial filter widths: 0.9 mm for μ and 1.5 mm for ξ (Delgorio et al.,
171 2021).

172
173
174
175
176
177
178
179
180
181
182
183
184
185
186
187
188
189
190
191
192
193

Figure 1 here

Memory Assessments

The memory battery included the California Verbal Learning Test III (CVLT) (Delis et al., 2017), Logical Memory (LM) from the Wechsler Memory Scale IV (Wechsler, 2009), and the spatial reconstruction (SR) task (Watson et al., 2013; Monti et al., 2014; Horecka et al., 2018). All participants completed the SR task (N = 88), while subsets of the participants also completed the CVLT (N = 73) and LM (N = 82) tasks.

California Verbal Learning Test: In the CVLT, the examiner read aloud a 16-word list (word list A) to participants a total of 5 times (i.e., trials). After each trial, participants recited the words they remembered back to the examiner. Participants were then read a second 16-word list (word list B) with semantically related items and were asked to recall as many of the words from this second word list that they could remember. Finally, participants asked to recall all the words they could remember from word list A. We calculated interference cost as the difference between recall of word list A, after the interference of word list B, and recall after the original fifth trial of word list A. Interference cost is an index of the loss of memory accuracy following mnemonic intrusions from semantically related items and has been associated with CA1-CA2 functional activation (Schlichting et al., 2014; Molitor et al., 2021). We also calculated delayed free recall score, which is the number of correct responses on word list A after a 30-minute delay.

194 **Logical Memory:** In the LM task, participants heard two short stories and were then asked to
195 recall everything they remember immediately after the examiner recites each story and again
196 after a delay period of 20-30 minutes. We calculated and analyzed the delayed free recall score
197 as the sum of correct responses on recalling details from both story A and story B after the delay,
198 which has previously been associated with SUB volumetric measures (Travis et al., 2014;
199 Zammit et al., 2017).

200

201 **Spatial Reconstruction:** The SR task involved participants studying the locations of five abstract
202 shapes for 20 seconds, which then disappear for four seconds and reappear at the top of the
203 screen where participants are instructed to arrange the shapes based on how they remember the
204 studied display (Watson et al., 2013; Monti et al., 2014). Performance on this task is determined
205 by errors in object placement including displacements, edge resizing, rearrangement, and
206 position swaps (Watson et al., 2013), from which we calculate the composite performance SR
207 error score by combining standardized z-scores of each error metric; we have used the composite
208 metric in our previous studies of MRE structure-function relationships (Schwarb et al., 2016,
209 2017; Daugherty et al., 2020). The SR error score was then converted ($1 - \text{SR error}$), such that
210 higher numbers are indicative of better task performance. SR performance has previously been
211 associated with DG-CA3 viscoelasticity (Daugherty et al., 2020), and relational memory and
212 pattern separation have been related to DG- CA3 functional activation (Yassa et al., 2011; Azab
213 et al., 2014).

214

215 Statistical Analysis

216 We computed sample mean, standard deviation, skew, and kurtosis for each MRE
217 measure and behavioral outcome, and determined relationships between each variable, including
218 bivariate correlations between each memory performance measure and stiffness, μ , and damping
219 ratio, ξ , of each HCsf region. We detected outliers from the original raw datasets for both the
220 memory task measures and HCsf MRE measures using a cutoff of 2.0x interquartile range (IQR).
221 Outliers for each memory task measure were based on residuals from multiple regression
222 models, with HCsf, age, and sex as predictors. Outliers for the HCsf regions were based on the
223 mean distribution of the participant data. All outliers were removed for the relevant analyses
224 accordingly.

225 Due to multicollinearity present among our predictors, ridge regression was used to
226 investigate specific associations between the HCsf and each memory performance measure.
227 Ridge regression is an extension of a multiple linear regression that addresses the problem of
228 multicollinearity among independent variables, which is present in our HCsf MRE data
229 (Daugherty et al., 2020; Delgorio et al., 2021). When independent variables are highly correlated
230 to one another, parameters in linear regression become unstable (Daoud, 2018). Ridge regression
231 addresses this issue by removing the unbiased estimate restriction that linear regression has,
232 introducing a penalty term, 'k,' that decreases the size of the predictor variable coefficients. This
233 in turn reduces model complexity and the overall effect of multicollinearity. This allows the
234 model to consider the contribution of each independent predictor (i.e., HCsf region) more
235 accurately (Golam Kibria, 2003). To confirm the presence of multicollinearity between the HCsf
236 properties, we used multiple regression models to find the variance inflation factor (VIF)
237 (Johnston et al., 2018).

238 We performed the ridge regression using R (v4.1.0) and the statistical package ‘lmridge
239 (v1.2)’ (Ullah et al., 2018). For each memory measure, all HCsf regions were included as
240 predictors of performance in one ridge regression model, with age and sex as additional predictor
241 variables. We standardized the predictor variables and used the function ‘kest’ to determine the
242 optimal ‘k’ based on the published literature. We chose the ‘MED’ equation for estimating ‘k’
243 (Golam Kibria, 2003) based on low mean square error and good performance on datasets with
244 high variance and large sample sizes (Muniz and Kibria, 2009; Muniz et al., 2012; Najarian et
245 al., 2013). For each ridge regression analysis, we considered the model R^2 , which represents the
246 cumulative variance explained by all the predictors in the model, and the individual coefficients,
247 which represent the unique effect each predictor attributes to the model outcomes.

248 Finally, we sought to consider whether HCsf properties influence the relationship
249 between age and memory performance, as both MRE properties and memory performance differ
250 with age. We used mediation models to examine whether the relationship between age and
251 memory performance may be mediated by HCsf μ and ξ , with one model tested for each memory
252 measure and associated HCsf region relationship (as determined in the previous analysis).
253 Mediation analyses were performed in Mplus (v8) (Muthén and Muthén, 2017); effect size and
254 95% confidence intervals not overlapping zero were interpreted as evidence of mediation (Hayes
255 and Scharkow, 2013).

256

257 **Results**

258 Outliers were removed for CVLT (interference cost and delayed free recall; $n = 2$), SR (n
259 = 2), and LM ($n = 4$) outcomes. Thus, our analyses were performed on the following final
260 sample sizes: CVLT ($N = 71$); LM ($N = 78$); SR ($N = 86$). Table 1 describes an overview of the

261 MRE measurement demographics for all participants, with demographics for the memory task
262 measures from the updated sample sizes without outliers.

263

264

Table 1 here

265

266 Correlations between HCsf, Memory, Age, and Sex

267 Bivariate correlations between the individual HCsf μ and ξ properties revealed the HCsf
268 were highly correlated with one another ($r > 0.7$). Additionally, all HCsf were significantly
269 related to age for both μ ($r > -0.47$) and ξ ($r > 0.47$). The relationship between sex and both DG-
270 CA3 and CA1-CA2 μ displayed small effect sizes ($d = 0.20$ and 0.36 , respectively), while the
271 SUB μ and sex relationship displayed a moderate effect size ($d = 0.56$). Similarly, the
272 relationship between sex and all HCsf ξ displayed small effect sizes ($d < 0.50$) (Table 2).
273 However, sex was included as a factor in analyses as MRE studies have shown sexual
274 dimorphism in brain mechanical properties and potentially different relationships with age
275 between males and females (Sack et al., 2009; Arani et al., 2015; Hiscox et al., 2020b). From all
276 multiple regression models, the VIF for DG-CA3 μ , CA1-CA2 μ , and all HCsf ξ were greater
277 than the threshold of 2.5 indicating multicollinearity, while the VIF of SUB μ was 2.2 and close
278 to the threshold (Johnston et al., 2018).

279

Table 2 here

280

281 Figure 2 shows correlations between μ of each HCsf region and performance on each
282 memory task, without controlling for age and sex. Each HCsf region μ (DG-CA3, CA1-CA2,
283 and SUB) correlated significantly with performance on memory tasks CVLT interference cost,

284 LM delayed free recall, and SR (all $p < 0.05$), with higher HCsf μ associating with better
285 memory performance, while only DG-CA3 μ correlated significantly with CVLT delayed free
286 recall. Figure 3 shows correlations between ξ of each HCsf region and performance on each
287 memory task, without controlling for age and sex. No significant correlations were present
288 between HCsf region ξ (DG-CA3, CA1-CA2, and SUB) and performance on CVLT interference
289 cost, CVLT delayed free recall, and LM delayed free recall ($p > 0.05$). For SR performance, all
290 HCsf ξ were significantly correlated ($p < 0.01$), with lower HCsf ξ associating with better
291 memory performance. Specific p and r values for each structure-function relationship are
292 indicated on each plot in Figures 2 and 3.

293 *Figure 2 here*

294 *Figure 3 here*

295

296 Age was also significantly related to CVLT interference cost performance ($r = -0.24$, $p =$
297 0.042), CVLT delayed free recall performance ($r = -0.37$, $p = 0.002$), LM delayed free recall
298 performance ($r = -0.34$, $p = 0.002$), and SR performance ($r = -0.66$, $p < 0.001$). Sex did not
299 display large effect sizes for any memory task measure ($d < 0.43$). Figures 4 and 5 display the
300 age correlations with all memory measures (Figure 4) and HCsf MRE measures (Figure 5).

301 *Figure 4 here*

302 *Figure 5 here*

303

304 *HCsf Structure-Function Relationships*

305 For each memory task measure, all HCsf regions were included as predictors in a ridge
306 regression model, along with age and sex. Table 3 presents a summary of the ridge regression

307 results for each stiffness-memory model, while Table 4 presents a summary of the ridge
308 regression results for each damping ratio-memory model. Each model description for both
309 Tables 3 and 4 included (1) the total model R^2 and (2) the individual predictor ridge estimators
310 ('b') and if they were significant in relation to the entire model. Statistically significant ridge
311 estimators indicate that specific predictors contributed a significantly larger effect to the overall
312 model variance compared to the other predictors.

313 **Stiffness-memory ridge regression models:** The optimal 'k' value for the CVLT
314 interference cost ridge regression model was 2.38. The overall R^2 was 0.033 and CA1-CA2 μ
315 was the only subfield region that significantly predicted task performance ($b = 0.90$, $p = 0.018$).
316 No other subfield was significant in the model ($p > 0.05$). The optimal 'k' value for CVLT
317 delayed free recall was 0.15. The overall R^2 was 0.169 and no HCsf μ were significant
318 contributors of CVLT delayed free recall performance, though age ($b = -10.1$, 0.002) and sex (b
319 $= 7.58$, $p = 0.010$) were both significant contributors. The optimal 'k' value for the LM delayed
320 free recall model was 0.89. The overall R^2 was 0.098 and both DG-CA3 μ ($b = 6.14$, $p = 0.016$)
321 and SUB μ ($b = 5.73$, $p = 0.032$) were the only significant predictors of delayed free recall
322 performance. The optimal 'k' value for the SR model was 0.072. The overall R^2 was 0.415 and
323 CA1-CA2 μ was the only significant subfield predictor of SR performance ($b = 2.32$, $p = 0.011$),
324 while the other subfield regions were not significant predictors ($p > 0.05$). Additionally, age was
325 a strong predictor of SR performance ($b = -4.17$, $p < 0.001$).

326

327

Table 3 here

328

329 **Damping ratio-memory ridge regression models:** For all models, no HCsf region
330 significantly predicted any memory performance measure ($p > 0.1$). However, age was a
331 significant contributor to CVLT delayed free recall performance ($b = -9.67, p < 0.001$), LM
332 delayed free recall performance ($b = -7.36, p = 0.005$), and SR performance ($b = -3.90, p <$
333 0.001). Sex was also a significant contributor to CVLT delayed free recall performance ($b =$
334 $5.73, p = 0.017$).

335

336

Table 4 here

337

338 We also considered individual HCsf volume as predictors of memory task performance as
339 HCsf volume is a common measure of tissue integrity and can be related to MRE measures of
340 tissue integrity. All HCsf volumes were corrected for head size (intracranial volume, ICV) using
341 the analysis of covariance (ANCOVA) approach, which corrects regional measures based on the
342 proportion of the difference between an individual's ICV and the average ICV for the sample
343 (Jack et al., 1989). Indeed, both DG-CA3 and CA1-CA2 exhibit significant correlations between
344 μ and volume ($p < 0.05$), but not SUB, while no HCsf exhibited significant correlations between
345 ξ and volume (Table 5).

346

Table 5 here

347

348 For each ridge regression models we included volume of each HCsf as predictors in
349 addition to HCsf μ , age, and sex, as before. Including these additional predictors did not change
350 the outcomes with μ of previously identified HCsf being the only significant predictors: CVLT
351 interference cost and CA1-CA2 μ ($p = 0.030$); LM delayed free recall and DG-CA3 μ ($p =$

352 0.009) and SUB μ ($p = 0.016$); and SR and CA-CA2 μ ($p = 0.009$). Table 6 presents complete
353 ridge regression results from the model including volume.

354 *Table 6 here*

355

356 *HCsf Stiffness as a Mediator of Age Effects on Memory Performance*

357 Based on the results from the ridge regression analyses, we performed individual
358 mediation models for each memory task to assess whether the individual HCsf stiffness
359 influenced the relationship between age and memory performance. Mediation models were
360 performed for each of the statistically significant HCsf stiffness-memory task relationships:
361 CA1-CA2 μ and CVLT interference cost, DG-CA3 μ and SUB μ and LM delayed free recall,
362 and CA1-CA2 μ and SR. Figure 6 illustrates the results for each model, including direct
363 relationships between each variable and the indirect mediated effect. CA1-CA2 μ significantly
364 mediates the effect of age on CVLT performance (*indirect* = -0.15, $p = 0.031$, 95% confidence
365 interval (CI) [-0.30, -0.02]), accounting for 62.4% of the total effect of age on performance. The
366 LM mediation model revealed that both DG-CA3 μ (*indirect* = -0.13, $p = 0.050$, 95% CI [-0.27, -
367 0.01]) and SUB μ (*indirect* = -0.13, $p = 0.054$, 95% CI [-0.27, -0.01]) have 95% CI that do not
368 overlap zero, supporting mediation that accounts for 39.8% and 39.5% of the total age effect
369 explained by DG-CA3 μ and SUB μ , respectively. However, it should be noted these effect sizes
370 are moderate and did not reach statistical significance. For the SR task, the model indicated that
371 CA1-CA2 μ did not mediate the relationship between age and performance (*indirect* = -0.099, p
372 = 0.073, 95% CI [-0.21, 0.01]), accounting for only 15.1% of the total age effect.

373

374 *Figure 6 here*

375

376 **Discussion**

377 Our goal was to identify if hypothesized unique associations existed between HCsf
378 viscoelasticity and specific memory domains across the adult lifespan. These results agree with
379 previous studies showing that while all HCsf are integral to good memory performance, each
380 region uniquely contributes to specific aspects of declarative memory encoding, recall, and
381 retrieval (Zeineh et al., 2003; Lee et al., 2004; Dimsdale-Zucker et al., 2018), which can be
382 observed with MRE. Our results complement previous MRE findings of strong structure-
383 function correlations between HC viscoelasticity and memory (Schwarb et al., 2016), as well as
384 dissociable relationships with other structures and functions, such as frontal cortex with fluid
385 intelligence and rule learning (Johnson et al., 2018; Schwarb et al., 2019). Our high-resolution
386 MRE approach allows us to identify structure-function dissociations between the small
387 neighboring HCsf for the first time, confirming the sensitivity of MRE measures to relevant
388 microstructural integrity in these regions, including that individual HCsf μ measures appear to be
389 stronger predictors of memory than volume measures.

390 We focused on three mnemonic processes associated with hippocampal function:
391 interference, delayed episodic recall, and relational memory. Previous volumetry and functional
392 MRI work has indicated that interference cost on traditional memory tasks is associated with
393 CA1-CA2 structure (Mueller et al., 2011; Molitor et al., 2021). Consistent with these findings,
394 we showed that CA1-CA2 μ was the strongest predictor for two types of memory performance:
395 recall following an interference and short-delay relational memory. CA1-CA2 is often associated
396 with delayed recall and memory consolidation (Mueller et al., 2011; Zammit et al., 2017). Some
397 studies suggest CA1 has a role in integrating related events with overlapping neural

398 representation, such as two similar word lists (Molitor et al., 2021) and match/mismatch
399 detection (Duncan et al., 2012; Schlichting et al., 2014). Additionally, prior work revealed
400 gradual, linear changes in CA1 activation when recalling semantically-related items or words
401 with increasing similarity (Leal and Yassa, 2018). Interference cost from the CVLT is a measure
402 of recall performance of a rehearsed list of words following presentation of an interference list,
403 which is consistent with the ability to detect differences between semantically-related items
404 (Kane and Engle, 2000), and thus supports the correlation with CA1-CA2 μ we observe here.
405 Prior imaging studies in older adults and dementia patients displayed similar correlations
406 between CA1 volume and delayed verbal recall (Kerchner et al., 2012; Zammit et al., 2017),
407 including CVLT delayed recall performance in cognitively impaired older adults (Mueller et al.,
408 2011). While interference cost is determined from immediate recall, there is potentially overlap
409 in strategies for both immediate and delayed recall on this task. Overall, the role of CA1 in
410 encoding and differentiating between related events as well as verbal recall performance support
411 the significant contribution of CA1-CA2 μ to resolving interference in memory recall.

412 Significant associations between SUB μ and LM task performance support prior work
413 that shows delayed episodic recall performance is associated with SUB volumetry (Travis et al.,
414 2014; Zammit et al., 2017). SUB is related to integrating and projecting information onto the
415 greater extra-hippocampal regions (O'Mara et al., 2009; Newmark et al., 2013; Travis et al.,
416 2014). Prior *in vivo* research showed associations between SUB volume and verbal free recall
417 (Hartopp et al., 2019), showcasing the important role of the SUB in recall after a delay. From the
418 tasks in this study, delayed episodic recall is also a standard measure for the CVLT; however,
419 there were no significant associations between CVLT delayed free recall and any HCsf μ
420 measure in the ridge regression analysis. These non-significant results are likely due to lack of

421 variability in the task measurement range for the sample, with most participants recalling many
422 words correctly.

423 Additionally, both functional MRI and MRE studies have shown that associative or
424 relational memory measures are related to DG-CA3 (Azab et al., 2014; Daugherty et al., 2020).
425 Relational memory is the ability to bind arbitrary information into a single representation (Cohen
426 and Eichenbaum, 1995; Eichenbaum and Cohen, 2004), which is critical to remembering story
427 details required in the LM task through deep encoding strategies to create associations among
428 details from the stories for recall after the delay (Wechsler, 2009). This is consistent with our
429 results showing LM performance was related to DG-CA3 μ . Neural signals from the DG-CA3 to
430 the SUB are conveyed via the tri-synaptic circuit (Duvernoy, 2005), and thus both structures
431 have a role in memory encoding. Specifically, DG-CA3 is thought to support associative
432 memory function and is related to encoding and subsequent recall of bound information (Berron
433 et al., 2016; Hainmueller and Bartos, 2020; Bouyeure et al., 2021).

434 Surprisingly, DG-CA3 μ was not associated with SR performance. SR is a relational
435 memory task (Monti et al., 2014; Horecka et al., 2018) that has been correlated with DG-CA3
436 viscoelastic measures in a young adult sample (Daugherty et al., 2020). In the current study, SR
437 performance was uniquely associated instead with CA1-CA2 μ and a smaller, non-significant
438 unique effect of DG-CA3. Age-related differences in CA1-CA2 structure are commonly reported
439 to be larger than in DG-CA3 (Daugherty et al., 2016), and the vulnerability of CA1-CA2 in
440 aging may account for its larger unique effect on SR performance here. SR requires encoding
441 from multiple objects and locations, as well as detecting errors when the participant places
442 objects during the reconstruction phase of the task (Watson et al., 2013; Monti et al., 2014;
443 Horecka et al., 2018). Therefore, the task plausibly requires the synchronous function of CA1

444 and DG-CA3 within the tri-synaptic circuit, where the DG granule and CA3 pyramidal cells
445 signal and transfer information to the CA1 pyramidal cells (Duvernoy, 2005). Indeed, strategies
446 for completing this task can engage similar processes as reflected by CVLT interference cost.
447 For instance, participants visually navigate the space with strategic viewing patterns that
448 influence later reconstruction performance on this task (Lucas et al., 2018); thus, potentially
449 influencing the firing rates observed in CA1-CA2. In pre-surgical epilepsy patients, differences
450 between CA1 and dorsolateral prefrontal cortex gamma power (an index of network activity)
451 predicted the precision of spatial memory judgments (Stevenson et al., 2018), which further
452 supports relational memory functions of CA1-CA2.

453 Aging affects both HCsf integrity and memory performance, and as such, examining age-
454 related differences can shed light on structure-function relationships in the brain. Our group
455 previously demonstrated that aging strongly affects HCsf viscoelasticity, and with differential
456 effects between HCsf (Delgorio et al., 2021). Thus, we also investigated the role of HCsf
457 viscoelasticity to partially account for age-related differences in memory performance. Of the
458 significant HCsf structure-function relationships observed in the ridge analysis, we found
459 evidence of CA1-CA2 μ strongly mediating the effect of age on CVLT performance, and
460 moderate effect sizes of both DG-CA3 μ and SUB μ mediating the effect on LM performance.
461 Overall, these results indicate that low HCsf μ contributes to worse memory performance with
462 age, which is consistent with previous findings using diffusion MRI methods (Hayek et al., 2020;
463 Radhakrishnan et al., 2020). Our data is cross-sectional, so our results from the mediation models
464 must be cautiously interpreted (Lindenberger et al., 2011), but these findings motivate future
465 longitudinal analyses.

466 There were several additional limitations present in our study. Relationships between
467 HCsf structure and function were observed with μ , but not ξ , despite previous studies reporting
468 relationships between memory performance and HC ξ , but not μ (Schwarb et al., 2016, 2017,
469 2019; Daugherty et al., 2020; Hiscox et al., 2020a). The reasons for this discrepancy are not
470 immediately clear, however, previous reports all studied narrow age ranges of either young or
471 older adults, while some included only male participants. This work included both male and
472 female adult participants across a large age range of 60 years. Examining our current sample
473 using subsets of participants in similar age ranges as those studies (i.e. < 35 years or > 65 years),
474 we did not observe any significant correlations between either HCsf μ or ξ and memory task
475 outcomes in either group, though these subsamples are smaller and less powered to detect such
476 effects, and a future study designed to understand how these structure-function relationships may
477 change across the lifespan is warranted. We note that in recent studies on pediatric participants,
478 MRE structure-function relationships were observed in μ but not ξ (McIlvain et al., 2020a,
479 2020b). We also recognize that this study shows weaker evidence of structure-function
480 dissociations than in our prior MRE work that reported a double dissociation in structure-
481 function relationships of relational memory and fluid intelligence performance with
482 viscoelasticity of the HC and orbitofrontal cortex (Johnson et al., 2018). This is due to the
483 memory functions examined here each depending on the HC as whole, in addition to being
484 particularly supported by individual HCsf, making dissociations more difficult to observe.

485 Here, we show through MRE metrics that the HCsf regions uniquely contribute to specific
486 memory task domains. These qualities make MRE a promising tool to track prodromal
487 neuropathology, improving differential diagnosis of dementia subtypes in the future. Future

488 studies will involve classifying similar structure-function relationships in patients with
489 Alzheimer's disease and mild cognitive impairment.

490

491 **References**

- 492 Arani A, Murphy MC, Glaser KJ, Manduca A, Lake DS, Kruse S, Jack Jr CR, Ehman R, Huston
493 J (2015) Measuring the effects of aging and sex on regional brain stiffness with MR
494 elastography in healthy older adults. *NeuroImage* 111:59–64.
- 495 Azab M, Stark SM, Stark CEL (2014) Contributions of human hippocampal subfields to spatial
496 and temporal pattern separation. *Hippocampus* 24:293–302.
- 497 Berron D, Schütze H, Maass A, Cardenas-Blanco A, Kuijf HJ, Kumaran D, Düzel E (2016)
498 Strong evidence for pattern separation in human dentate gyrus. *Journal of Neuroscience*
499 36:7569–7579.
- 500 Bouyeure A, Patil S, Mauconduit F, Poiret C, Isai D, Noulhiane M (2021) Hippocampal subfield
501 volumes and memory discrimination in the developing brain. *Hippocampus* 31:1202–1214.
- 502 Cohen NJ, Eichenbaum H (1995) *Memory, amnesia, and the hippocampal system*. MIT press.
- 503 Daoud JI (2018) *Multicollinearity and Regression Analysis*. In: *Journal of Physics: Conference*
504 *Series*. Institute of Physics Publishing.
- 505 Daugherty AM, Bender AR, Raz N, Ofen N (2016) Age differences in hippocampal subfield
506 volumes from childhood to late adulthood. *Hippocampus* 26:220–228.
- 507 Daugherty AM, Schwarb HD, McGarry MDJ, Johnson CL, Cohen NJ (2020) Magnetic
508 Resonance Elastography of Human Hippocampal Subfields: CA3-Dentate Gyrus
509 Viscoelasticity Predicts Relational Memory Accuracy. *Journal of Cognitive Neuroscience*
510 32:1704–1713.
- 511 de Flores R, la Joie R, Chételat G (2015) Structural imaging of hippocampal subfields in healthy
512 aging and Alzheimer's disease. *Neuroscience* 309:29–50.
- 513 Delgorio PL, Hiscox LV, Daugherty AM, Sanjana F, Pohlig RT, Ellison JM, Martens CR,
514 Schwarb H, McGarry MDJ, Johnson CL (2021) Effect of Aging on the Viscoelastic
515 Properties of Hippocampal Subfields Assessed with High-Resolution MR Elastography.
516 *Cerebral Cortex* 31:2799–2811.
- 517 Delis DC, Kramer JH, Kaplan E, Ober BA (2017) *The California Verbal Learning Test-3* (3rd
518 ed.). Psychological Corporation.
- 519 Dimsdale-Zucker HR, Ritchey M, Ekstrom AD, Yonelinas AP, Ranganath C (2018) CA1 and
520 CA3 differentially support spontaneous retrieval of episodic contexts within human
521 hippocampal subfields. *Nature Communications* 9:1–8.
- 522 Duncan K, Ketz N, Inati SJ, Davachi L (2012) Evidence for area CA1 as a match/mismatch
523 detector: A high-resolution fMRI study of the human hippocampus. *Hippocampus* 22:389–
524 398.
- 525 Duvernoy HM (2005) *The human hippocampus: functional anatomy, vascularization and serial*
526 *sections with MRI*. Springer Science & Business Media.
- 527 Eichenbaum H, Cohen NJ (2004) *From conditioning to conscious recollection: Memory systems*
528 *of the brain*. Oxford University Press on Demand.

529 Foster CM, Kennedy KM, Hoagey DA, Rodrigue KM (2019) The role of hippocampal subfield
530 volume and fornix microstructure in episodic memory across the lifespan. *Hippocampus*
531 29:1206–1223.

532 Golam Kibria BM (2003) Performance of some New Ridge regression estimators.
533 *Communications in Statistics Part B: Simulation and Computation* 32:419–435.

534 Golomb J, Kluger A, de Leon MJ, Ferris SH, Mittelman MP, Cohen J, George AE (1996)
535 Hippocampal formation size predicts declining memory performance in normal aging.
536 *Neurology* 47:810–813.

537 Hainmueller T, Bartos M (2020) Dentate gyrus circuits for encoding, retrieval and discrimination
538 of episodic memories. *Nature Reviews Neuroscience* 21:153–168.

539 Hannum AJ, McIlvain G, Sowinski D, McGarry MDJ, Johnson CL (2021) Correlated noise in
540 brain magnetic resonance elastography. *Magnetic Resonance in Medicine* 87:1313–1328.

541 Hartopp N, Wright P, Ray NJ, Evans TE, Metzler-Baddeley C, Aggleton JP, O’Sullivan MJ
542 (2019) A key role for subiculum–fornix connectivity in recollection in older age. *Frontiers*
543 *in Systems Neuroscience* 12:70.

544 Hayek D, Thams F, Flöel A, Antonenko D (2020) Dentate Gyrus Volume Mediates the Effect of
545 Fornix Microstructure on Memory Formation in Older Adults. *Frontiers in Aging*
546 *Neuroscience* 12:79.

547 Hayes AF, Scharkow M (2013) The relative trustworthiness of inferential tests of the indirect
548 effect in statistical mediation analysis: does method really matter? *Psychol Sci* 24:1918–
549 1927.

550 Hiscox LV, Johnson CL, Barnhill E, McGarry MDJ, Huston J, van Beek EJR, Starr JM, Roberts
551 N (2016) Magnetic resonance elastography (MRE) of the human brain: Technique, findings
552 and clinical applications. *Physics in Medicine and Biology* 61:R401–R437.

553 Hiscox LV, Johnson CL, McGarry MDJ, Perrins M, Littlejohn A, van Beek EJR, Roberts N,
554 Starr JM (2018) High-resolution magnetic resonance elastography reveals differences in
555 subcortical gray matter viscoelasticity between young and healthy older adults.
556 *Neurobiology of Aging* 65:158–167.

557 Hiscox LV, Johnson CL, McGarry MDJ, Schwarb H, van Beek EJR, Roberts N, Starr JM
558 (2020a) Hippocampal viscoelasticity and episodic memory performance in healthy older
559 adults examined with magnetic resonance elastography. *Brain Imaging Behav* 14:175–185.

560 Hiscox LV, McGarry MDJ, Schwarb H, van Houten EEW, Pohlig RT, Roberts N, Huesmann
561 GR, Burzynska AZ, Sutton BP, Hillman CH, Kramer AF, Cohen NJ, Barbey AK, Paulsen
562 KD, Johnson CL (2020b) Standard-space atlas of the viscoelastic properties of the human
563 brain. *Human Brain Mapping* 41:5282–5300.

564 Hiscox LV, Schwarb H, McGarry MDJ, Johnson CL (2021) Aging brain mechanics: Progress
565 and promise of magnetic resonance elastography. *NeuroImage* 232:117889.

566 Horecka KM, Dulas MR, Schwarb H, Lucas HD, Duff M, Cohen NJ (2018) Reconstructing
567 relational information. *Hippocampus* 28:164–177.

568 Jack CR, Twomey CK, Zinsmeister AR, Sharbrough FW, Petersen RC, Cascino GD, Fws N
569 (1989) Anterior temporal lobes and hippocampal formations: normative volumetric
570 measurements from MR images in young adults. *Radiology* 172:549–554.

571 Jenkinson M, Beckmann CF, Behrens TEJ, Woolrich MW, Smith SM (2012) Fsl. *NeuroImage*
572 62:782–790.

573 Johnson CL, Holtrop JL, Anderson AT, Sutton BP (2016a) Brain MR elastography with
574 multiband excitation and nonlinear motion-induced phase error correction. In: *Proceedings*

575 of the 24th Annual Meeting of the International Society for Magnetic Resonance in
576 Medicine, pp 1951.

577 Johnson CL, Schwarb H, Horecka KM, McGarry MDJ, Hillman CH, Kramer AF, Cohen NJ,
578 Barbey AK (2018) Double dissociation of structure-function relationships in memory and
579 fluid intelligence observed with magnetic resonance elastography. *NeuroImage* 171:99–106.

580 Johnson CL, Schwarb H, McGarry MDJ, Anderson AT, Huesmann GR, Sutton BP, Cohen NJ
581 (2016b) Viscoelasticity of subcortical gray matter structures. *Human Brain Mapping*
582 37:4221–4233.

583 Johnston R, Jones K, Manley D (2018) Confounding and collinearity in regression analysis: a
584 cautionary tale and an alternative procedure, illustrated by studies of British voting
585 behaviour. *Quality and Quantity* 52:1957–1976.

586 Kane MJ, Engle RW (2000) Working-memory capacity, proactive interference, and divided
587 attention: limits on long-term memory retrieval. *Journal of Experimental Psychology:*
588 *Learning, Memory, and Cognition* 26:336.

589 Kerchner GA, Deutsch GK, Zeineh M, Dougherty RF, Saranathan M, Rutt BK (2012)
590 Hippocampal CA1 apical neuropil atrophy and memory performance in Alzheimer’s
591 disease. *NeuroImage* 63:194–202.

592 Leal SL, Yassa MA (2018) Integrating new findings and examining clinical applications of
593 pattern separation. *Nature Neuroscience* 21:163–173.

594 Lee I, Rao G, Knierim JJ (2004) A Double Dissociation between Hippocampal Subfields:
595 Differential Time Course of CA3 and CA1 Place Cells for Processing Changed
596 Environments. *Neuron* 42:803–815.

597 Lindenberger U, von Oertzen T, Ghisletta P, Hertzog C (2011) Cross-Sectional Age Variance
598 Extraction: What’s Change Got To Do With It? *Psychology and Aging* 26:34–47.

599 Lucas HD, Duff MC, Cohen NJ (2018) The hippocampus promotes effective saccadic
600 information gathering in humans. *Journal of Cognitive Neuroscience* 31:186–201.

601 McGarry MDJ, Johnson CL, Sutton BP, van Houten EEW, Georgiadis JG, Weaver JB, Paulsen
602 KD (2013) Including spatial information in nonlinear inversion MR elastography using soft
603 prior regularization. *IEEE Trans Med Imaging* 32:1901–1909.

604 McGarry MDJ, van Houten EEW, Johnson CL, Georgiadis JG, Sutton BP, Weaver JB, Paulsen
605 KD (2012) Multiresolution MR elastography using nonlinear inversion. *Medical Physics*
606 39:6388–6396.

607 McGarry MDJ, van Houten EEW, Perrinez PR, Pattison AJ, Weaver JB, Paulsen KD (2011) An
608 octahedral shear strain-based measure of SNR for 3D MR elastography. *Physics in*
609 *Medicine & Biology* 56:N153.

610 McIlvain G, Clements RG, Magoon EM, Spielberg JM, Telzer EH, Johnson CL (2020a)
611 Viscoelasticity of reward and control systems in adolescent risk taking. *NeuroImage*
612 215:116850.

613 McIlvain G, Tracy JB, Chaze CA, Petersen DA, Villermaux GM, Wright HG, Miller F,
614 Crenshaw JR, Johnson CL (2020b) Brain Stiffness Relates to Dynamic Balance Reactions
615 in Children With Cerebral Palsy. *Journal of Child Neurology* 35:463–471.

616 Molitor RJ, Sherril KR, Morton NW, Miller AA, Preston AR (2021) Memory reactivation during
617 learning simultaneously promotes dentate gyrus/CA2, 3 pattern differentiation and CA1
618 memory integration. *Journal of Neuroscience* 41:726–738.

619 Monti JM, Cooke GE, Watson PD, Voss MW, Kramer AF, Cohen NJ (2014) Relating
620 hippocampus to relational memory processing across domains and delays. *J Cogn Neurosci*
621 27:234–245.

622 Morrison JH, Hof PR (1997) Life and death of neurons in the aging brain. *Science* (1979)
623 278:412–419.

624 Mueller SG, Chao LL, Berman B, Weiner MW (2011) Evidence for functional specialization of
625 hippocampal subfields detected by MR subfield volumetry on high resolution images at 4T.
626 *NeuroImage* 56:851–857.

627 Mueller SG, Stables L, Du AT, Schuff N, Truran D, Cashdollar N, Weiner MW (2007)
628 Measurement of hippocampal subfields and age-related changes with high resolution MRI
629 at 4 T. *Neurobiology of Aging* 28:719–726.

630 Muniz G, Kibria BM, Shukur G (2012) On Developing Ridge Regression Parameters: A
631 Graphical Investigation. Department of Mathematics and Statistics 10 Available at:
632 https://digitalcommons.fiu.edu/math_fac/10.

633 Muniz G, Kibria BMG (2009) On some ridge regression estimators: An empirical comparisons.
634 *Communications in Statistics: Simulation and Computation* 38:621–630.

635 Murphy MC, Huston J, Ehman RL (2019) MR elastography of the brain and its application in
636 neurological diseases. *NeuroImage* 187:176–183.

637 Muthén B, Muthén L (2017) *Mplus*. Chapman and Hall/CRC.

638 Najarian S, Arashi M, Kibria BMG (2013) A simulation study on some restricted ridge
639 regression estimators. *Communications in Statistics: Simulation and Computation* 42:871–
640 890.

641 Newmark RE, Schon K, Ross RS, Stern CE (2013) Contributions of the hippocampal subfields
642 and entorhinal cortex to disambiguation during working memory. *Hippocampus* 23:467–
643 475.

644 O’Mara SM, Sanchez-Vives MV, Brotons-Mas JR, O’Hare E (2009) Roles for the subiculum in
645 spatial information processing, memory, motivation and the temporal control of behaviour.
646 *Progress in Neuro-Psychopharmacology and Biological Psychiatry* 33:782–790.

647 Petersen RC, Jack CR, Xu Y-C, Waring SC, O’Brien PC, Smith GE, Ivnik RJ, Tangalos EG,
648 Boeve BF, Kokmen E (2000) Memory and MRI-based hippocampal volumes in aging and
649 AD. *Neurology* 54:581.

650 Radhakrishnan H, Stark SM, Stark CEL (2020) Microstructural Alterations in Hippocampal
651 Subfields Mediate Age-Related Memory Decline in Humans. *Frontiers in Aging*
652 *Neuroscience* 12:94.

653 Sack I, Beierbach B, Wuerfel J, Klatt D, Hamhaber U, Papazoglou S, Martus P, Braun J (2009)
654 The impact of aging and gender on brain viscoelasticity. *NeuroImage* 46:652–657.

655 Sack I, Jöhrens K, Würfel J, Braun J (2013) Structure-sensitive elastography: On the viscoelastic
656 powerlaw behavior of in vivo human tissue in health and disease. *Soft Matter* 9:5672–5680.

657 Sanjana F, Delgorio PL, Hiscox LV, DeConne TM, Hobson JC, Cohen ML, Johnson CL,
658 Martens CR (2021) Blood lipid markers are associated with hippocampal viscoelastic
659 properties and memory in humans. *Journal of Cerebral Blood Flow and Metabolism*
660 41:1417–1427.

661 Schlichting ML, Zeithamova D, Preston AR (2014) CA1 subfield contributions to memory
662 integration and inference. *Hippocampus* 24:1248–1260.

663 Schwarb H, Johnson CL, Daugherty AM, Hillman CH, Kramer AF, Cohen NJ, Barbey AK
664 (2017) Aerobic fitness, hippocampal viscoelasticity, and relational memory performance.
665 *NeuroImage* 153:179–188.

666 Schwarb H, Johnson CL, Dulas MR, McGarry MDJ, Holtrop JL, Watson PD, Wang JX, Voss
667 JL, Sutton BP, Cohen NJ (2019) Structural and Functional MRI Evidence for Distinct
668 Medial Temporal and Prefrontal Roles in Context-dependent Relational Memory. *J Cogn
669 Neurosci* 31:1857–1872.

670 Schwarb H, Johnson CL, McGarry MDJ, Cohen NJ (2016) Medial temporal lobe viscoelasticity
671 and relational memory performance. *NeuroImage* 132:534–541.

672 Stevenson RF, Zheng J, Mnatsakanyan L, Vadera S, Knight RT, Lin JJ, Yassa MA (2018)
673 Hippocampal CA1 gamma power predicts the precision of spatial memory judgments. *Proc
674 Natl Acad Sci U S A* 115:10148–10153.

675 Travis SG, Huang Y, Fujiwara E, Radomski A, Olsen F, Carter R, Seres P, Malykhin N v. (2014)
676 High field structural MRI reveals specific episodic memory correlates in the subfields of the
677 hippocampus. *Neuropsychologia* 53:233–245.

678 Ullah MI, Aslam M, Altaf S (2018) *lmridge: A Comprehensive R Package for Ridge Regression.*
679 *R J* 10:326.

680 Watson PD, Voss JL, Warren DE, Tranel D, Cohen NJ (2013) Spatial reconstruction by patients
681 with hippocampal damage is dominated by relational memory errors. *Hippocampus* 23:570–
682 580.

683 Wechsler D (2009) *WMS-IV: Wechsler memory scale.* Pearson.

684 West MJ (1993) Regionally specific loss of neurons in the aging human hippocampus. *Neurobiol
685 Aging* 14:287–293.

686 Wisse LEM, Biessels GJ, Heringa SM, Kuijf HJ, Luijten PR, Geerlings MI, Group UVCIVCIS
687 (2014) Hippocampal subfield volumes at 7T in early Alzheimer’s disease and normal aging.
688 *Neurobiol Aging* 35:2039–2045.

689 Yassa MA, Lacy JW, Stark SM, Albert MS, Gallagher M, Stark CEL (2011) Pattern separation
690 deficits associated with increased hippocampal CA3 and dentate gyrus activity in
691 nondemented older adults. *Hippocampus* 21:968–979.

692 Yushkevich PA, Pluta JB, Wang H, Xie L, Ding SL, Gertje EC, Mancuso L, Kliot D, Das SR,
693 Wolk DA (2015) Automated volumetry and regional thickness analysis of hippocampal
694 subfields and medial temporal cortical structures in mild cognitive impairment. *Human
695 Brain Mapping* 36:258–287.

696 Zammit AR, Ezzati A, Zimmerman ME, Lipton RB, Lipton ML, Katz MJ (2017) Roles of
697 hippocampal subfields in verbal and visual episodic memory. *Behavioural Brain Research*
698 317:157–162.

699 Zeineh MM, Engel SA, Thompson PM, Bookheimer SY (2003) Dynamics of the Hippocampus
700 During Encoding and Retrieval of Face-Name Pairs. *Science* (1979) 299:577–580.

701

702

703

704 **Data Availability**

705 Data is available upon request.

706

707 **Figure Legends**

708 **Figure 1:** Overview of the HCsf-specific high-resolution MRE protocol. (A) In step one, we
709 applied 50 Hz micron-level vibrations with a Resoundant pneumatic actuator via a passive head
710 pillow driver. (B) In step two, we used a 1.25mm isotropic resolution multiband, multishot MRE
711 sequence to image the shear waves generated in (A). (C) In steps three and four, we first used
712 ASHS to segment the HCsf regions of interest (DG-CA3, CA1-CA2, and SUB) and then used
713 NLI to generate measurements of shear stiffness for each HCsf region (Delgorio et al., 2021).

714

715 **Figure 2:** Overview of simple bivariate correlations between HCsf regional μ and memory
716 performance measures (not correcting for age and sex). Correlations observed between each
717 HCsf region and CVLT III interference cost performance (A-C) and delayed free recall
718 performance (D-F). Correlations observed between each HCsf region and logical memory
719 delayed free recall performance (G-I). Correlations observed between each HCsf region and SR
720 performance (J-L). (* $p < 0.05$; ** $p < 0.01$; *** $p < 0.001$).

721

722 **Figure 3:** Overview of simple bivariate correlations between HCsf regional ξ and memory
723 performance measures (not correcting for age and sex). Correlations observed between each
724 HCsf region and CVLT III interference cost performance (A-C) and delayed free recall
725 performance (D-F). Correlations observed between each HCsf region and logical memory

726 delayed free recall performance (G-I). Correlations observed between each HCsf region and SR
727 performance (J-L). (* $p < 0.01$; ** $p < 0.001$).

728
729 **Figure 4:** Summary of bivariate correlations between memory measures and age. (A) CVLT
730 interference cost performance and age were significantly related ($r = -0.24$, $p = 0.042$). (B)
731 CVLT delayed free recall performance and age were significantly related ($r = -0.37$, $p = 0.002$).
732 (C) LM delayed free recall performance and age were significantly related ($r = -0.34$, $p = 0.002$).
733 (D) SR performance and age were significantly related ($r = -0.66$, $p < 0.001$).

734
735 **Figure 5:** Summary of bivariate correlations between HCsf MRE measures and age. (A-C)
736 Bivariate correlations between HCsf μ and age. All regions were significantly related to age ($p <$
737 0.001). (D-F) Bivariate correlations between HCsf ξ and age. All regions were significantly
738 related to age ($p < 0.01$).

739
740 **Figure 6:** Mediation results for all memory task models. (A) **CVLT:** CA1-CA2 μ significantly
741 mediates the relationship between age and interference cost (indirect = -0.15 , $p = 0.031$). (B and
742 C) **Logical Memory:** Both DG-CA3 μ (indirect = -0.13 , $p = 0.050$) and SUB μ (indirect = -0.13 ,
743 $p = 0.054$) models have 95% CI that do not overlap zero, supporting mediation, although the
744 effect sizes do not reach statistical significance. Together this indicates DG-CA3 μ and SUB μ
745 may have a moderate influence on logical memory performance across the lifespan. (D) **Spatial**
746 **Reconstruction:** CA1-CA2 μ does not mediate the effect of age on SR (indirect = -0.099 , $p =$
747 0.073) in this sample.

748

749

750 **Tables**

751 **Table 1: Participant Demographics and Distribution of MRE and Memory Outcome**
 752 **Measures**

Category	Measure	Mean (SD)	Min/Max	S	K
Demographics	Age (years)	59.7 (15.8)	23.0/81.0	-1.12	0.23
MRE μ (kPa)	DG-CA3	3.21 (0.45)	1.63/4.20	-0.63	1.10
	CA1-CA2	3.28 (0.42)	1.89/4.24	-0.35	0.38
	SUB	2.97 (0.46)	1.73/4.03	-0.39	-0.16
MRE ξ	DG-CA3	0.21 (0.04)	0.14/0.30	0.43	-0.03
	CA1-CA2	0.19 (0.03)	0.12/0.27	0.08	-0.60
	SUB	0.15 (0.04)	0.09/0.24	0.58	-0.40
Memory Tasks	<i>CVLT III:</i> Interference Cost	-1.49 (1.67)	-6.00/2.00	-0.44	0.01
	<i>CVLT III:</i> Delayed Free Recall	11.4 (3.54)	1.0/16.0	-0.62	-0.06
	<i>Logical Memory:</i> Delayed Free Recall	24.7 (5.95)	12.0/40.0	0.15	-0.17
	<i>Spatial Reconstruction</i>	0.06 (0.84)	-1.69/1.43	-0.32	-0.75

753 |S|: skewness, |K|: kurtosis, < or > 1.96 for |S| and |K| indicate a violation of the assumption of normality
 754

755 **Table 1:** Overview of the participant demographics, including sample age distribution, MRE μ
 756 and ξ distribution for all HCsf regions, and memory task distribution for each task.
 757

758

759

760

761 **Table 2: Summary of Bivariate Correlation Coefficients for all HCsf Regional MRE**
 762 **measures, Age, and Sex**

Bivariate Correlations for HCsf μ			
	DG-CA3 μ	CA1-CA2 μ	SUB μ
DG-CA3 μ	-		
CA1-CA2 μ	0.86*	-	
SUB μ	0.71*	0.74*	-
Age	-0.47*	-0.56*	-0.51*
Sex [†]	0.20	0.36	0.56
Bivariate Correlations for HCsf ξ			
	DG-CA3 ξ	CA1-CA2 ξ	SUB ξ
DG-CA3 ξ	-		
CA1-CA2 ξ	0.89*	-	
SUB ξ	0.83*	0.87*	-
Age	0.47*	0.58*	0.52*
Sex [†]	0.25	0.43	0.50

763 * $p < 0.001$

764 [†] This row contains Cohen's d effect sizes

765
 766 **Table 2:** Summary of bivariate correlations between all HCsf regional MRE measures, age, and
 767 sex. Correlations between the HCsf μ showed that all regions were significantly correlated to one
 768 another ($p < 0.001$). Additionally, all HCsf μ were also significantly related to age ($p < 0.001$).
 769 There were small effect sizes in the relationships between sex and DG-CA3 ($d = 0.20$) and CA1-
 770 CA2 μ ($d = 0.36$), while the relationship between sex and SUB μ displayed a medium effect size
 771 ($d = 0.56$). Correlations between the HCsf ξ showed that all regions were significantly correlated
 772 to one another ($p < 0.001$). Additionally, all HCsf ξ were also significantly related to age ($p <$
 773 0.001). There were small effect sizes in the relationships between sex and all HCsf ξ ($d < 0.5$).
 774

775 **Table 3: Overview of the ridge regression results for each memory task model, including**
 776 **HCsf μ . b and p-values are given for each predictor variable.**

	CVLT III: Interference Cost		CVLT III: Delayed Free Recall		Logical Memory: Delayed Free Recall		Spatial Reconstruction	
	R ²	k-value	R ²	k-value	R ²	k-value	R ²	k-value
Results	b-weight	p-value	b-weight	p-value	b-weight	p-value	b-weight	p-value
Age	-0.66	0.135	-10.1	0.002**	-5.26	0.065	-4.17	< 0.001***
Sex	0.01	0.984	7.58	0.010*	0.58	0.842	0.55	0.362
DG-CA3 μ	0.74	0.055	3.66	0.293	6.14	0.016*	-0.69	0.423
CA1-CA2 μ	0.90	0.018*	-2.11	0.550	2.82	0.239	2.32	0.011*
SUB μ	0.67	0.10	0.76	0.823	5.73	0.032*	-0.51	0.516

* $p < 0.05$, ** $p < 0.01$, *** $p < 0.001$

777
 778
 779 **Table 3:** Overview of the ridge regression results for each memory task, HCsf μ model. **CVLT**
 780 **Interference Cost:** CA1-CA2 μ was the only significant HCsf predictor of interference cost
 781 performance (b = 0.90, p = 0.018). **CVLT Delayed Free Recall:** There were no significant HCsf
 782 μ predictors of CVLT delayed free recall performance. Age (b = -10.1, p = 0.002) and sex (b =
 783 7.58, p = 0.010) were the only significant predictors of task performance. **Logical Memory:**
 784 Both DG-CA3 μ (b = 6.14, p = 0.016) and SUB μ (b = 5.73, p = 0.032) were significant HCsf
 785 predictors of logical memory delayed free recall performance. **Spatial Reconstruction:** CA1-
 786 CA2 μ was the only significant HCsf predictor of spatial reconstruction performance (b = 2.32, p
 787 = 0.011). Age was also a significant predictor for this task (b = -4.17, p < 0.001).
 788
 789
 790
 791
 792
 793
 794
 795
 796
 797
 798
 799
 800
 801

802 **Table 4: Overview of the ridge regression results for each memory task model, including**
 803 **HCsf ξ . b and p-values are given for each predictor variable.**

	CVLT III: Interference Cost		CVLT III: Delayed Free Recall		Logical Memory: Delayed Free Recall		Spatial Reconstruction	
	R ²	k-value	R ²	k-value	R ²	k-value	R ²	k-value
Results	b-weight	p-value	b-weight	p-value	b-weight	p-value	b-weight	p-value
Age	-1.31	0.104	-9.67	< 0.001***	-7.36	0.005**	-3.90	< 0.001***
Sex	0.04	0.962	5.73	0.017*	-0.57	0.832	0.46	0.401
DG-CA3 ξ	-0.44	0.502	0.15	0.948	-1.73	0.401	0.38	0.528
CA1-CA2 ξ	-0.47	0.417	0.58	0.775	1.28	0.488	-0.85	0.147
SUB ξ	-0.62	0.349	1.62	0.478	-1.41	0.498	-0.28	0.655

* $p < 0.05$, ** $p < 0.01$, *** $p < 0.001$

804
 805
 806 **Table 4: Overview of the ridge regression results for each memory task, HCsf ξ model. CVLT**
 807 **Interference Cost:** There were no significant HCsf ξ predictors of CVLT interference cost
 808 performance. **CVLT Delayed Free Recall:** There were no significant HCsf ξ predictors of
 809 CVLT delayed free recall performance. Age (b = -9.67, p < 0.001) and sex (b = 5.73, p = 0.017)
 810 were the only significant predictors of task performance. **Logical Memory:** There were no
 811 significant HCsf ξ predictors of logical memory delayed free recall performance. Age was the
 812 only significant predictor of logical memory delayed free recall performance (b = -7.36, p =
 813 0.005). **Spatial Reconstruction:** There were no significant HCsf ξ predictors of spatial
 814 reconstruction performance. Age was the only significant predictor of logical memory delayed
 815 free recall performance (b = -3.90, p < 0.001).

816
 817
 818
 819
 820
 821
 822
 823
 824
 825
 826
 827
 828
 829

830 **Table 5: Correlations between HCsf MRE measures, μ and ξ , with HCsf volume.**

	DG-CA3	CA1-CA2	SUB
μ vs. volume	0.36***	0.51***	0.05
ξ vs. volume	-0.13	-0.17	0.004

831 *** $p < 0.001$

832 **Table 5:** Summary of bivariate correlations between all HCsf regional MRE measures, μ and ξ ,
 833 with HCsf volume. Correlations between the HCsf μ and volume measures showed that both
 834 DG-CA3 and CA1-CA2 μ were significantly correlated with DG-CA3 and CA1-CA2 volume,
 835 respectively ($p < 0.001$). SUB μ and volume were not significantly correlated ($p > 0.6$).
 836 Correlations between the HCsf ξ and volume measures showed that all regions were not
 837 significantly correlated to one another ($p > 0.1$).

838
 839
 840
 841
 842
 843
 844
 845
 846
 847
 848
 849
 850
 851
 852
 853
 854
 855
 856
 857
 858
 859
 860
 861
 862
 863
 864
 865
 866

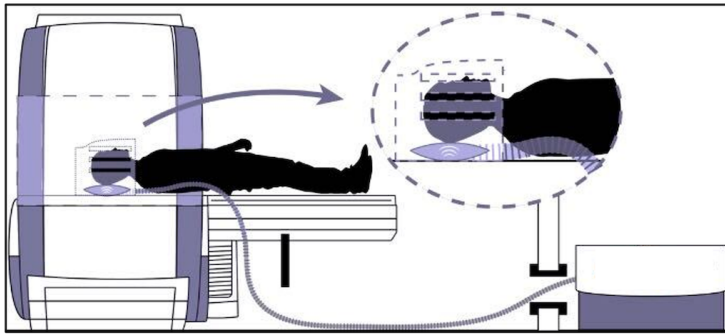
867 **Table 6: Overview of the ridge regression results for each memory task model, including**
 868 **both HCsf μ and volume. b and p-values are given for each predictor variable.**

	CVLT III: Interference Cost		CVLT III: Delayed Free Recall		Logical Memory: Delayed Free Recall		Spatial Reconstruction	
	R ²	k-value	R ²	k-value	R ²	k-value	R ²	k-value
Results	b-weight	p-value	b-weight	p-value	b-weight	p-value	b-weight	p-value
Age	-0.92	0.232	-6.40	0.003**	-4.24	0.071	-2.81	< 0.001***
Sex	0.06	0.944	5.06	0.016*	0.705	0.774	0.391	0.394
DG-CA3 μ	0.963	0.153	2.29	0.220	5.51	0.009**	0.059	0.892
CA1-CA2 μ	1.38	0.030*	0.164	0.926	2.06	0.278	1.11	0.009**
SUB μ	0.842	0.239	0.629	0.746	5.35	0.016*	0.156	0.732
DG-CA3 volume	0.206	0.774	2.51	0.200	-1.73	0.427	-0.007	0.988
CA1-CA2 volume	-0.035	0.959	-1.17	0.533	3.24	0.123	0.761	0.086
SUB volume	-0.565	0.475	-1.30	0.529	4.08	0.092	0.553	0.231

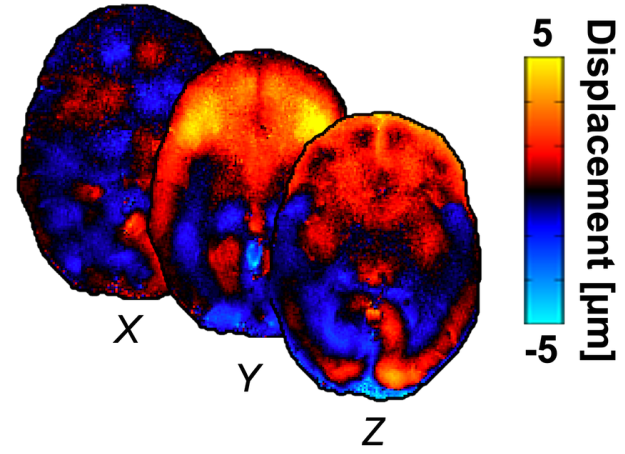
869 * $p < 0.05$, ** $p < 0.01$, *** $p < 0.001$

870
 871 **Table 6:** Overview of the ridge regression results for each memory task, HCsf μ model,
 872 including HCsf volume. **CVLT Interference Cost:** CA1-CA2 μ was the only significant HCsf
 873 predictor of interference cost performance (b = 1.38, p = 0.030). There were no significant HCsf
 874 volume predictors of interference cost performance. **CVLT Delayed Free Recall:** There were no
 875 significant HCsf μ and volume predictors of CVLT delayed free recall performance. Age (b = -
 876 6.40, p = 0.003) and sex (b = 5.06, p = 0.016) were the only significant predictors of task
 877 performance. **Logical Memory:** Both DG-CA3 μ (b = 5.51, p = 0.009) and SUB μ (b = 5.35, p =
 878 0.016) were significant HCsf predictors of logical memory delayed free recall performance.
 879 There were no significant HCsf volume predictors of logical memory delayed free recall
 880 performance **Spatial Reconstruction:** CA1-CA2 μ was the only significant HCsf predictor of
 881 spatial reconstruction performance (b = 1.11, p = 0.009). Age was also a significant predictor for
 882 this task (b = -2.81, p < 0.001). There were no significant HCsf volume predictors of spatial
 883 reconstruction performance.

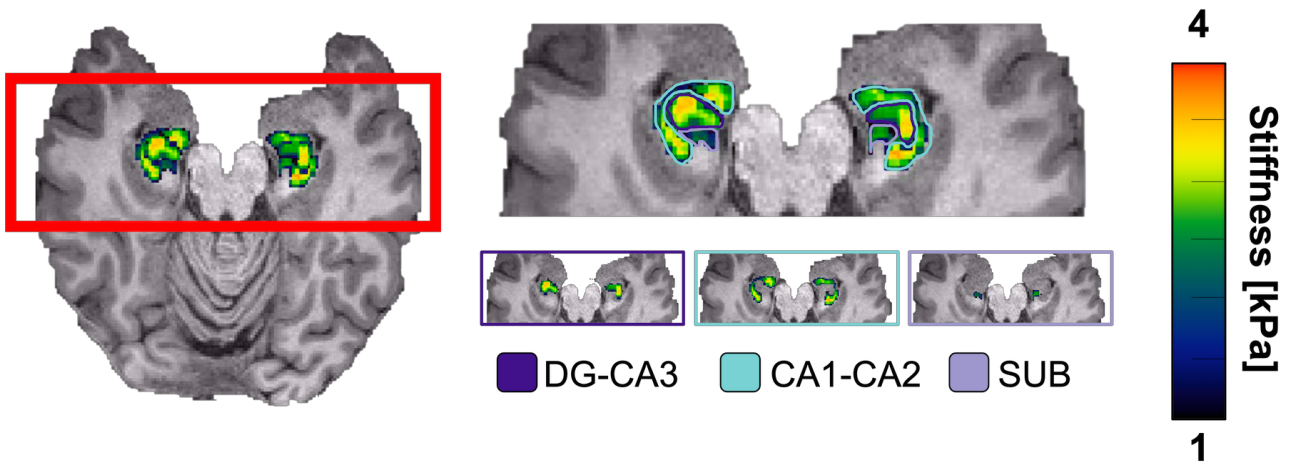
(A)



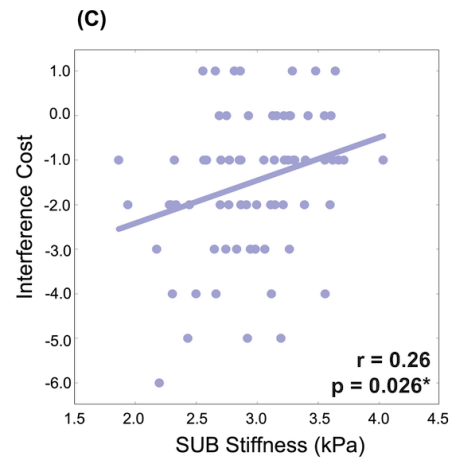
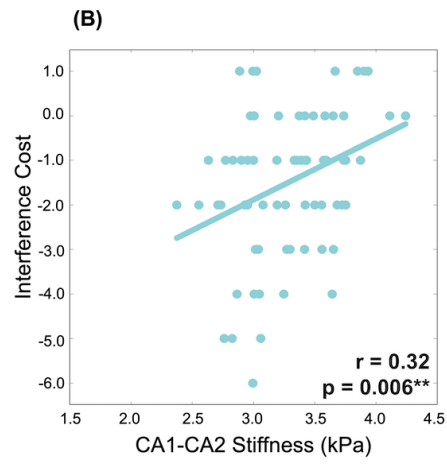
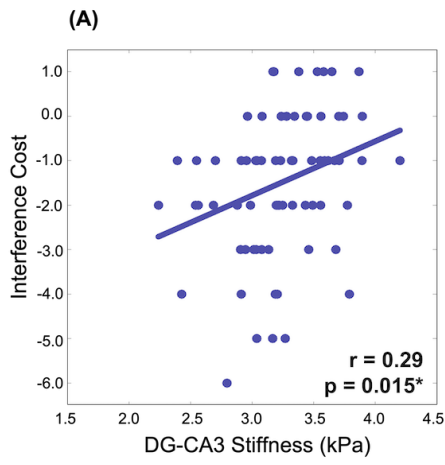
(B)



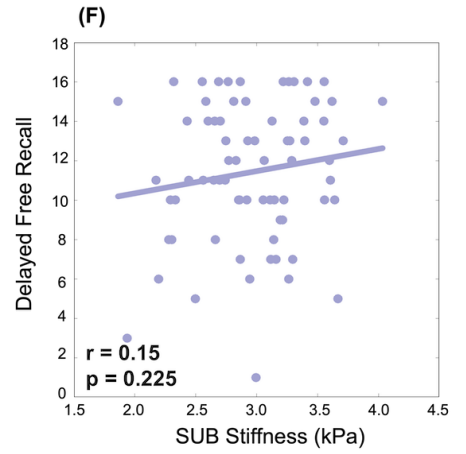
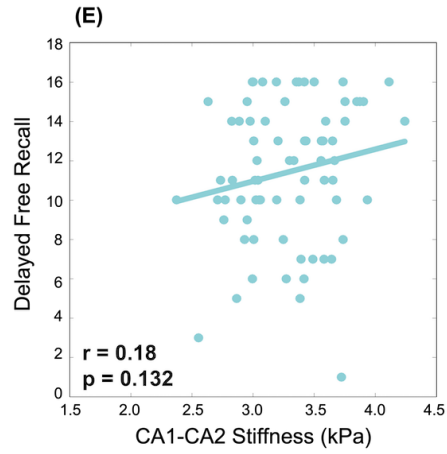
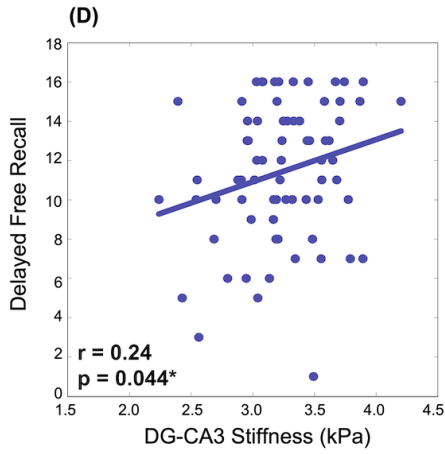
(C)



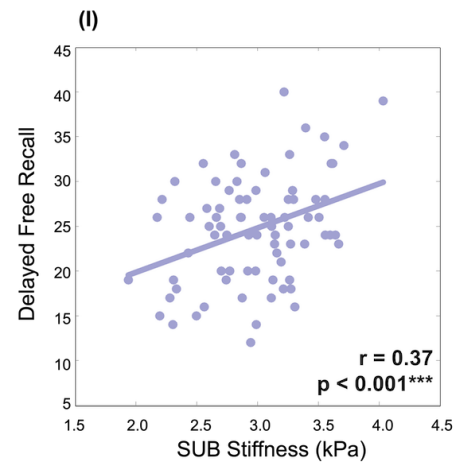
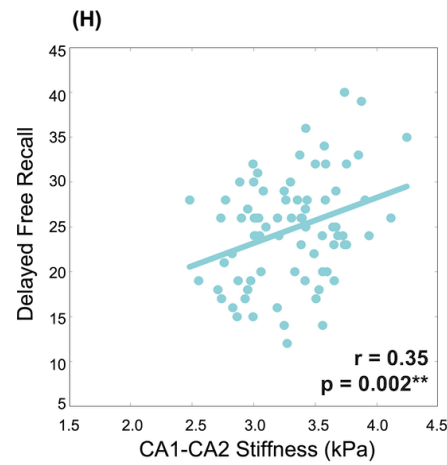
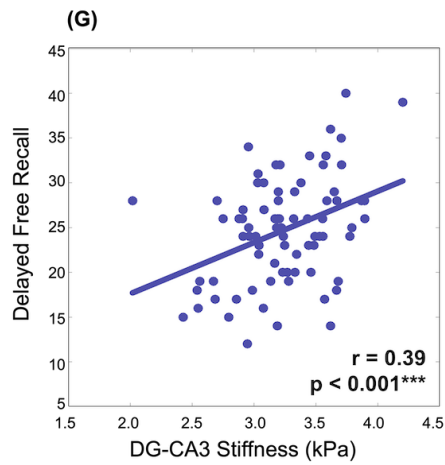
CVLT III: Interference Cost



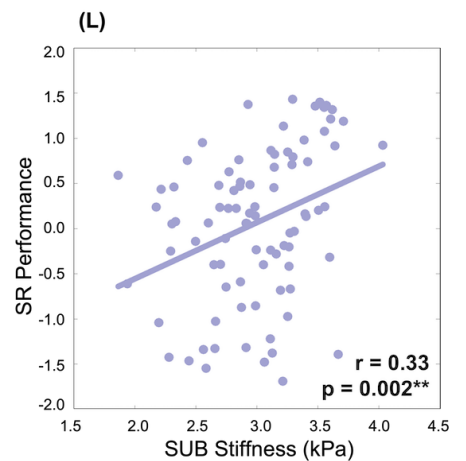
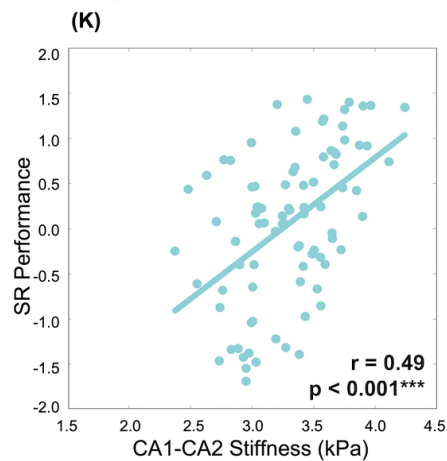
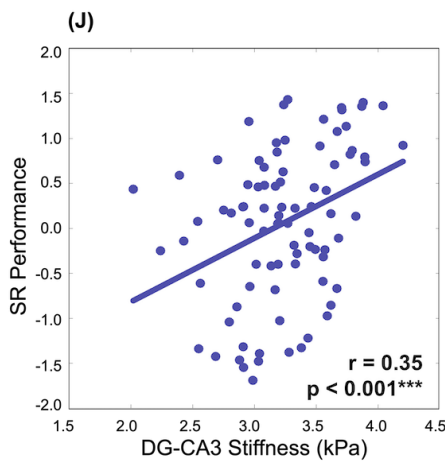
CVLT III: Delayed Free Recall



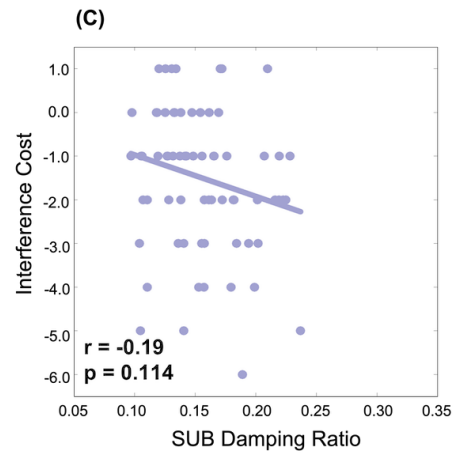
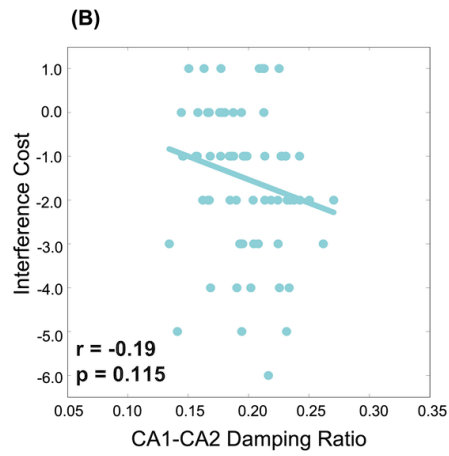
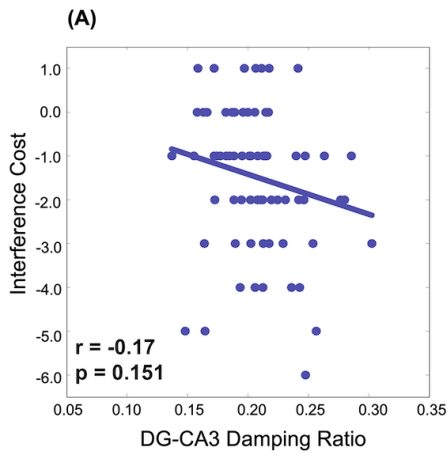
Logical Memory: Delayed Free Recall



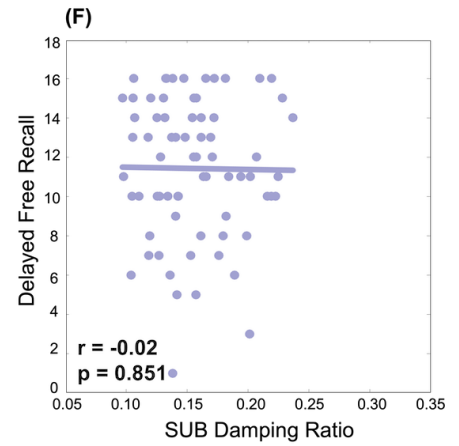
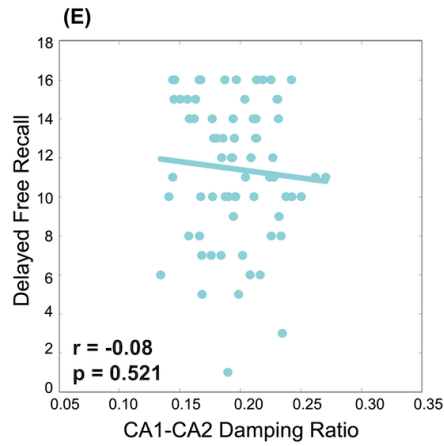
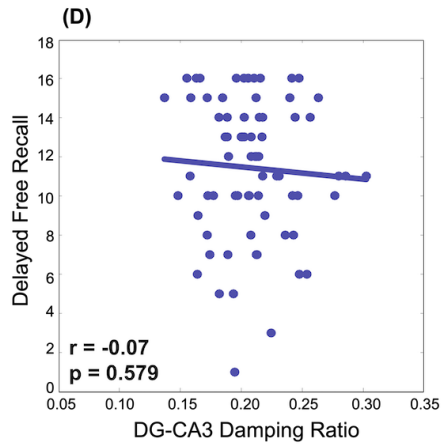
Spatial Reconstruction



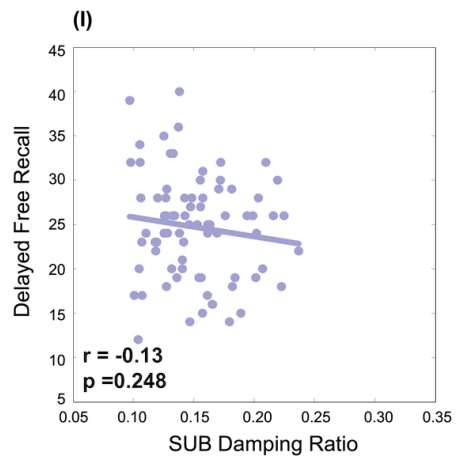
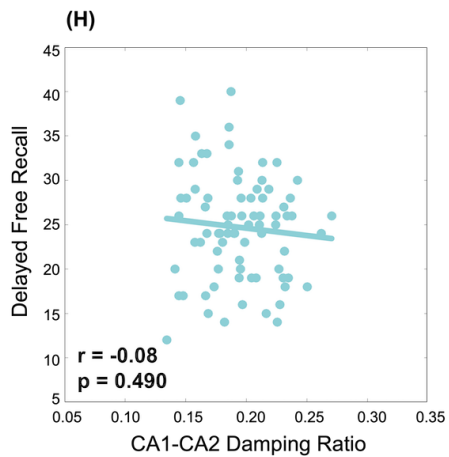
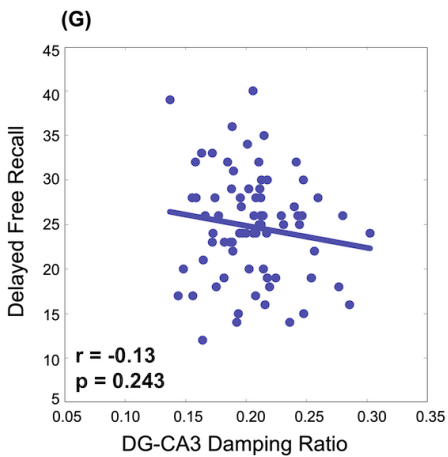
CVLT III: Interference Cost



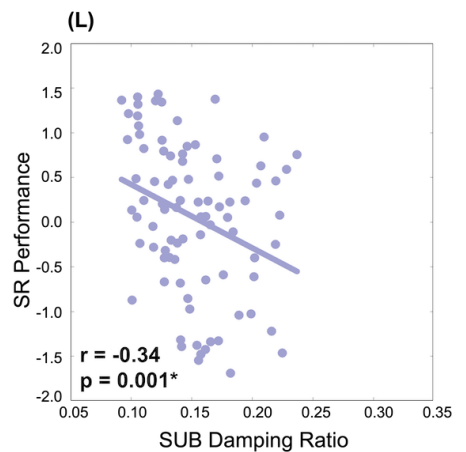
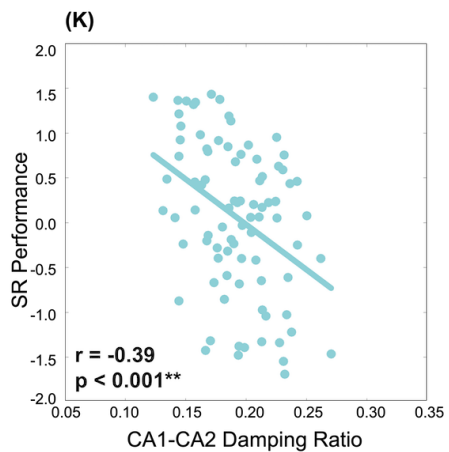
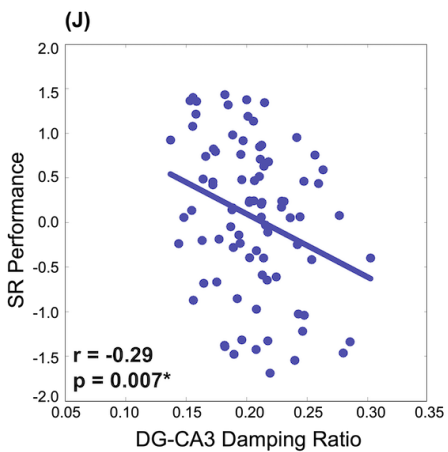
CVLT III: Delayed Free Recall



Logical Memory: Delayed Free Recall

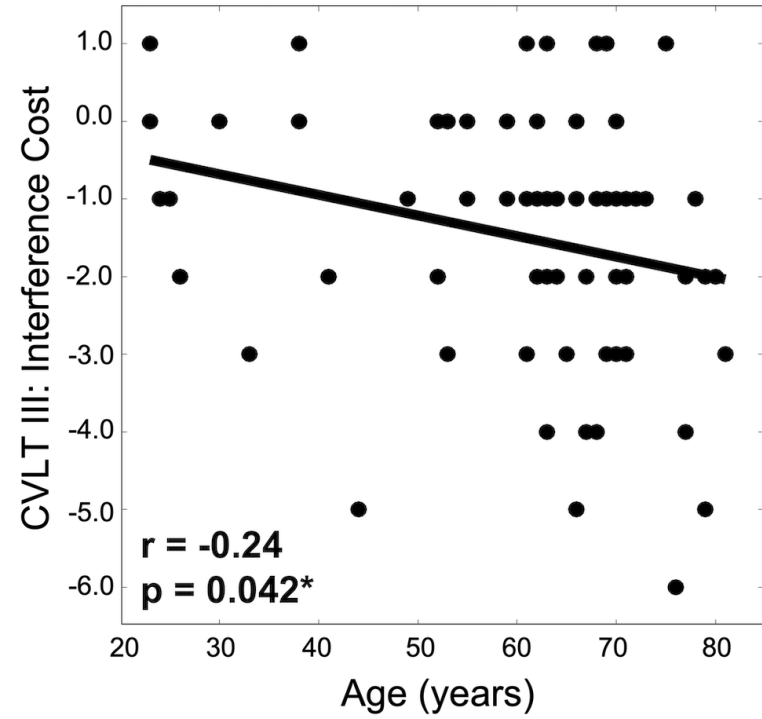


Spatial Reconstruction

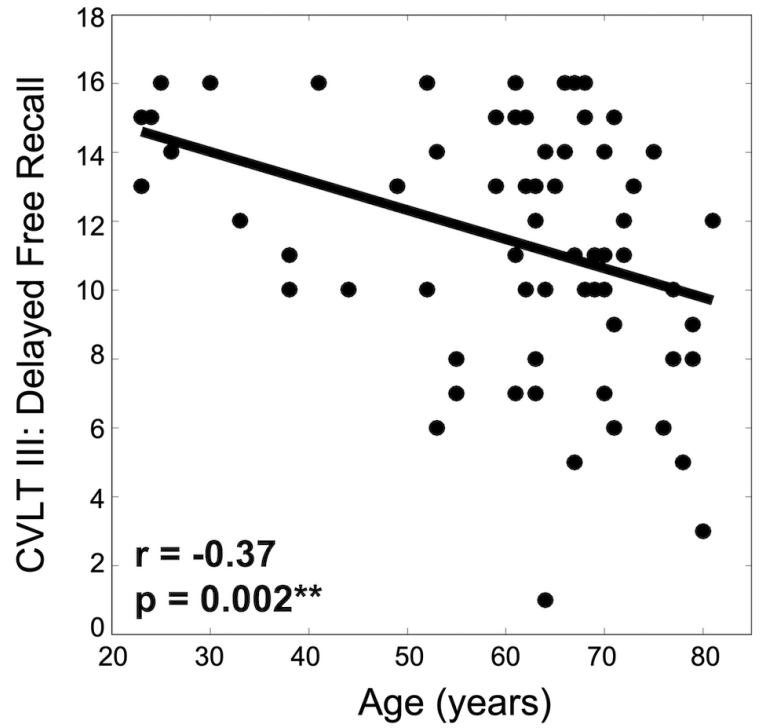


Memory Task Performance vs. Age

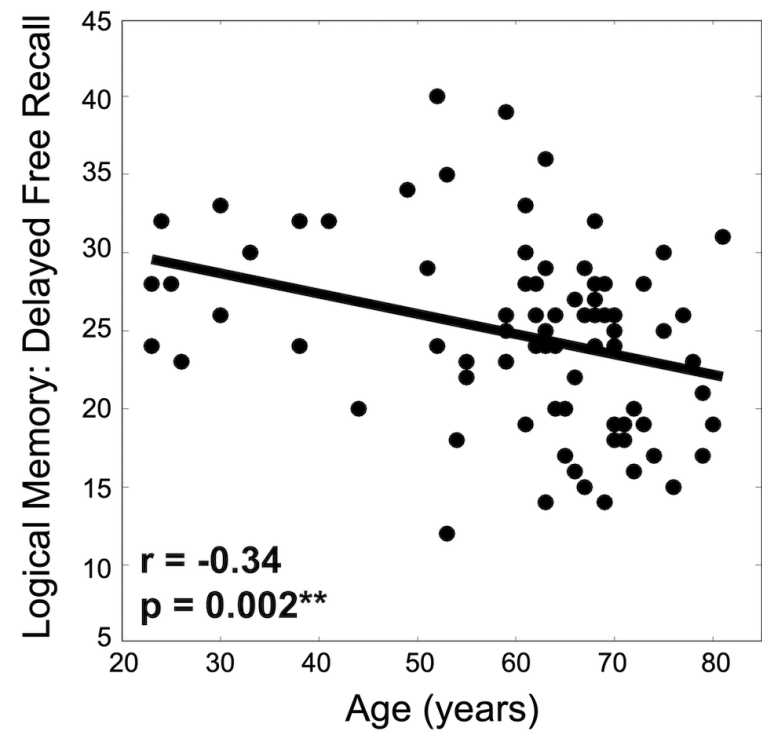
(A)



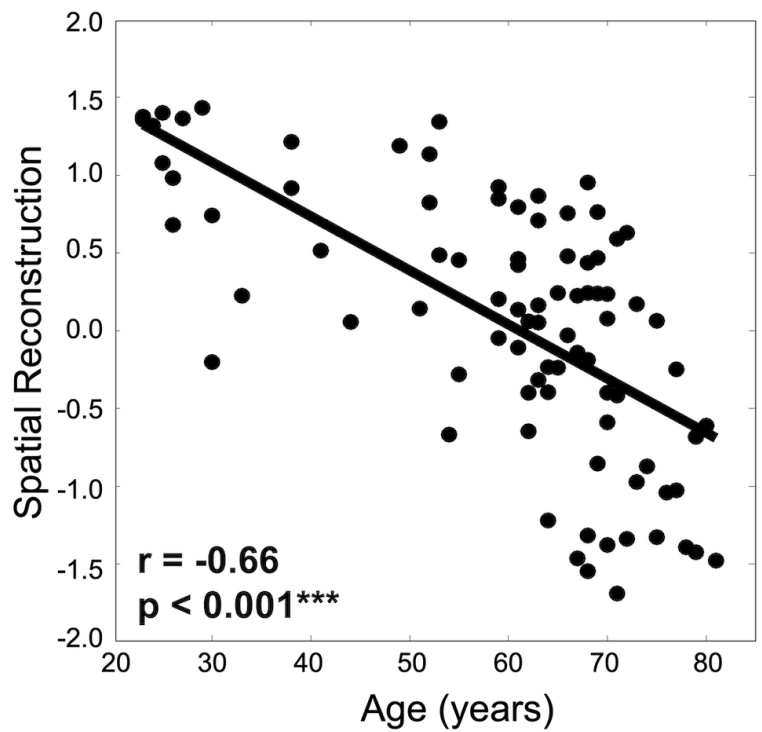
(B)



(C)

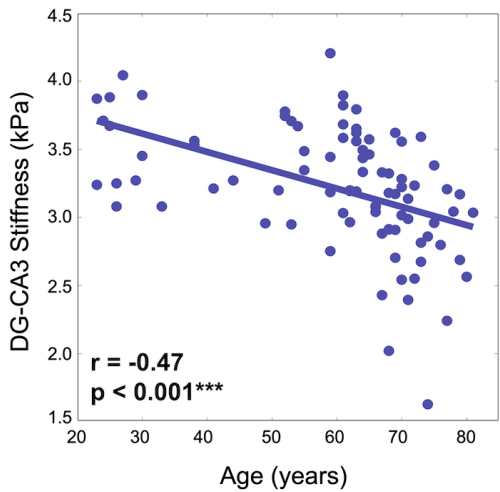


(D)

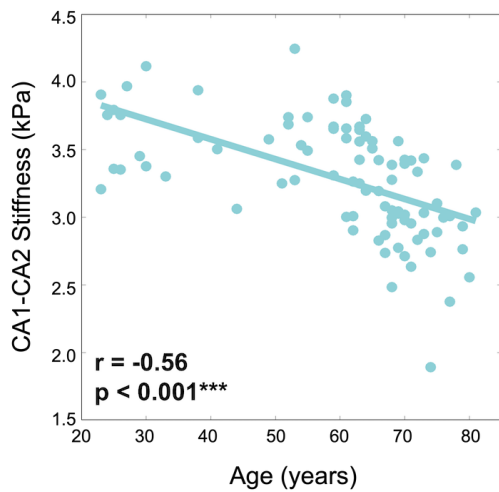


HCsf μ vs. Age

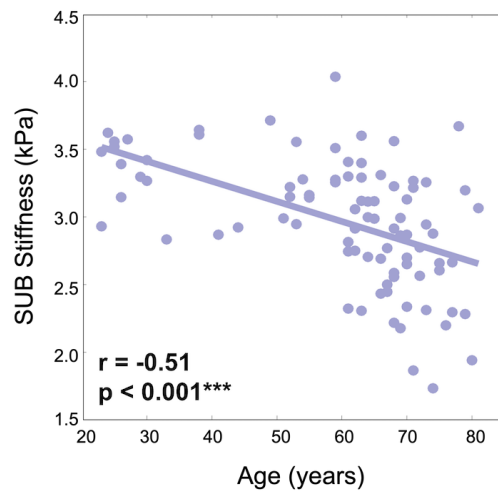
(A)



(B)

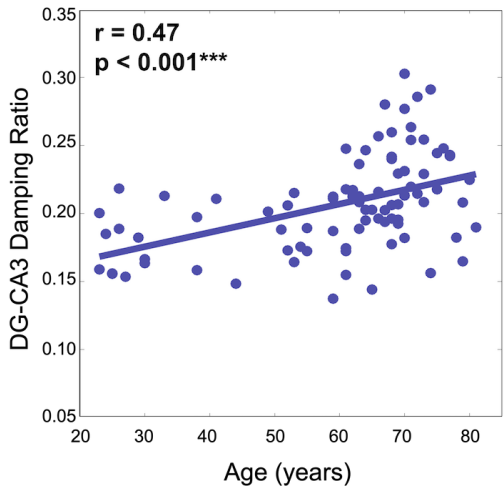


(C)

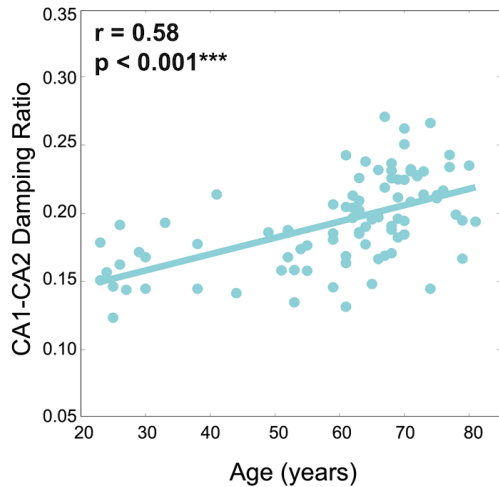


HCsf ξ vs. Age

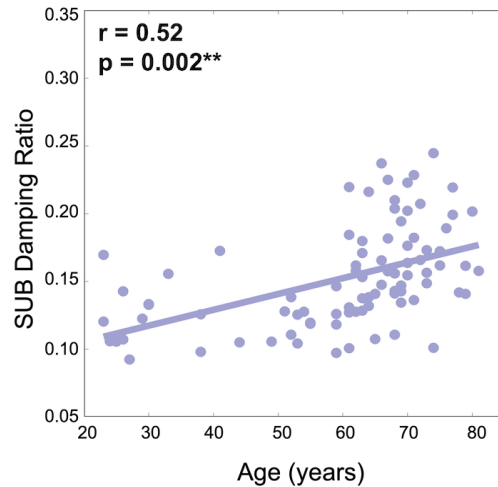
(D)



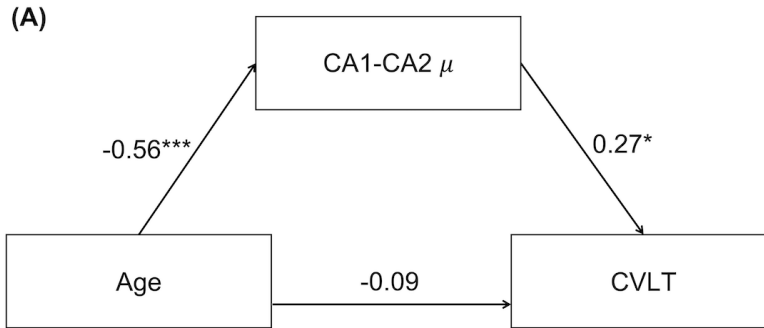
(E)



(F)

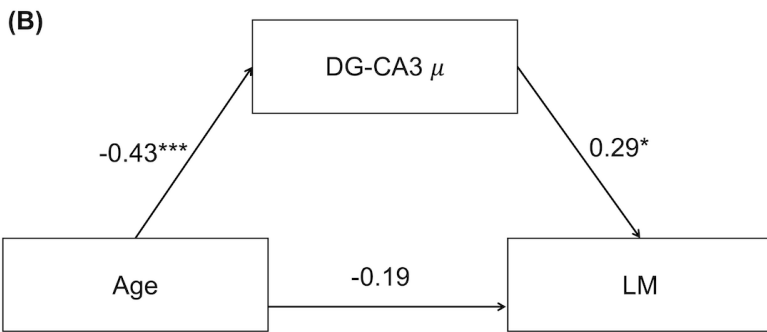


CVLT III: Interference Cost

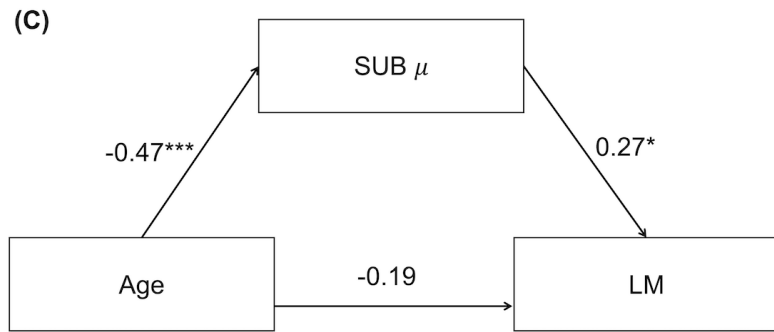


Indirect Effect: -0.15^* ($p = 0.031$); 95% CI $[-0.30, -0.02]$

Logical Memory: Delayed Free Recall

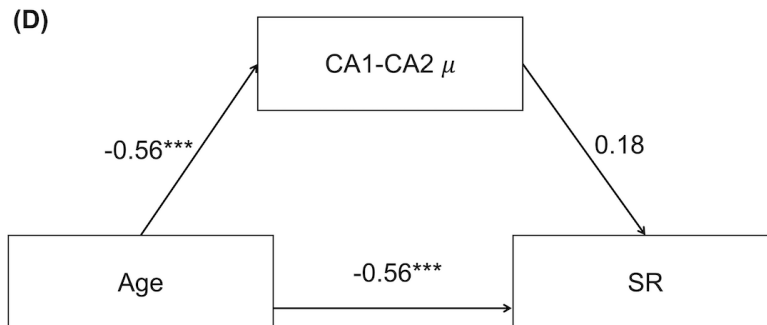


Indirect Effect: -0.13 ($p = 0.050$); 95% CI $[-0.27, -0.01]$



Indirect Effect: -0.13 ($p = 0.054$); 95% CI $[-0.27, -0.01]$

Spatial Reconstruction



Indirect Effect: -0.099 ($p = 0.073$); 95% CI $[-0.21, 0.01]$